JACS
JOURNAL OF THE AMERICAN CHEMICAL SOCIETY

ARTICLE

pubs.acs.org/JACS

Low-Bandgap Donor−Acceptor Conjugated Polymer Sensitizers for Dye-Sensitized Solar Cells

Zhen Fang, Aaron A. Eshbaugh, and Kirk S. Schanze*

Department of Chemistry and Center for Macromolecular Science and Engineering University of Florida, P.O. Box 117200, Gainesville, Florida 32611-7200, United States

Supporting Information

ABSTRACT: A set of two donor−acceptor type conjugated polymers with carboxylic acid side groups have been synthesized and utilized as active materials for dye-sensitized solar cells (DSSCs). The polymers feature a π-conjugated backbone consisting of an electron-poor 2,1,3-benzothiadiazole (BTD, acceptor) unit, alternating with either a thiophene−fluorene−thiophene triad (**2a**) or a terthiophene (**3a**) segment as the donor. The donor−acceptor polymers absorb broadly throughout the visible region, with terthiophene−BTD polymer **3a** exhibiting an absorption onset at approximately 625 nm corresponding to a ∼1.9 eV bandgap. The polymers adsorb onto the surface of nanostructured TiO_2 due to interaction of the polar carboxylic acid units with the metal oxide surface. The resulting films absorb visible light strongly, and their spectra approximately mirror the polymers' solution absorption. Interestingly, a series of samples of **3a** with different molecular weight (M_n) adsorb to TiO_2 to an extent that varies inversely with M_n. DSSCs that utilize the donor−acceptor polymers as sensitizers were tested using an I^-/I_3^- electrolyte. Importantly, for the set of polymer sensitizers **3a** with varying M_n, the DSSC efficiency varies inversely with M_n, a result that reflects the difference in adsorption efficiency observed in the film absorption experiments. The best DSSC cell tested is based on a sample of **3a** with $M_n \sim 4000$, and it exhibits a ∼65% peak IPCE with J_{sc} ∼12.6 mA cm^{-2} under AM1.5 illumination and an overall power conversion efficiency of ∼3%.

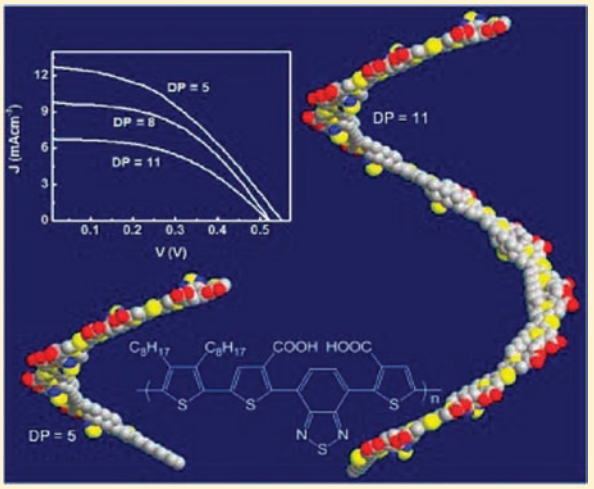

INTRODUCTION

Dye-sensitized solar cells (DSSCs) have received considerable attention as a low-cost alternative to conventional inorganic solid state solar cells.[1,2] The advantages of the DSSC format include its use of relatively low-cost materials and the possibility that mechanically flexible and aesthetically pleasing modules can be developed and deployed on a large scale for relatively low overall cost. A typical DSSC features a working electrode constructed from a mesoporous TiO_2 film that is sensitized by a small molecule chromophore. Most often, the light-absorbing sensitizer is based on a transition metal complex that features a metal-to-ligand charge transfer excited state. Specific metal complex sensitizers have been developed that exhibit excellent absorption throughout the visible and near-infrared regions and give rise to DSSCs exhibiting >85% incident photon to current efficiency (IPCE) over a broad region of the solar spectrum.[3] More recently, a number of highly efficient small molecule organic chromophores have also been developed that are based on charge transfer transitions across conjugated donor−acceptor (D-A) type chromophores.[4,5]

Conjugated polyelectrolytes (CPEs) are π-conjugated polymers that feature strong or weakly acidic (or basic) solubilizing groups such as carboxylic or alkyl sulfonic acids. CPEs feature effective light-harvesting efficiency because of their relatively large absorption coefficients and tunable optical bandgaps.[6] The ability to control the highest occupied molecular orbital (HOMO) and lowest unoccupied molecular orbital (LUMO) levels of CPEs allows one to design and synthesize low bandgap polymers that exhibit broad absorption throughout the visible and into the near-IR regions, potentially leading to high light-harvesting efficiency and charge injection efficiency at the interface of a wide-bandgap semiconductor. Previous work from our group and others has demonstrated that using specific CPEs functionalized with carboxylic acid units serve as effective sensitizers in DSSCs with relatively high IPCE and moderate power conversion efficiency.[7−12]

Although the overall efficiency of CPE-based DSSCs remains lower as compared to cells based on metal complexes and organic dyes,[3−5] a substantial opportunity exists for DSSC efficiency optimization by taking advantage of the ability to use molecular

Received: November 4, 2010
Published: February 09, 2011

Chart 1. Structures of 1, 2a, and 3a-DPs

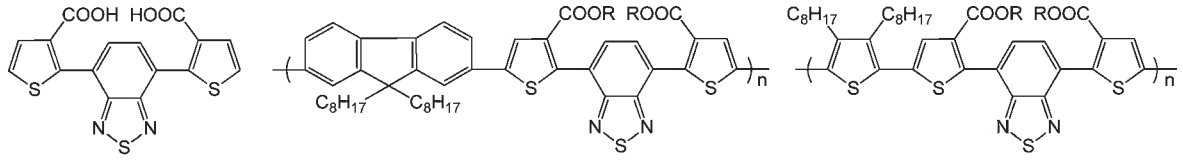

design and synthesis to engineer specific polymer structures that are optimized for light harvesting and exciton and charge transport. Specifically, the design and synthesis of alternating D-A copolymers have seen significant development in the past several years in the context of developing low bandgap materials with broad and intense absorption throughout the visible and near-IR spectral regions.[13] These materials have been the subject of much interest for application in organic solar cells and photodetectors. However, there have been few if any groups who have explored the application of low-bandgap D-A conjugated polymer systems in the DSSC format.[14]

In the present article, we detail the synthesis and characterization of two structurally similar carboxylic acid-substituted D-A type polymers, **2a** and **3a**-DP (where DP represents the degree of polymerization (DP), Chart 1) and explore their use as sensitizers in TiO_2 DSSCs. In these polymers, the electron-poor 2,1,3-benzothiadiazole (BTD) unit serves as the acceptor, while either a thiophene−fluorene−thiophene triad (**2a**) or a terthiophene segment (**3a**-DP) acts as the donor. These polymers offer specific advantages when they are applied as the light-absorbing sensitizers in DSSCs. First, the alternating D-A structure leads to charge separation in the excited state, and this may facilitate charge injection into TiO_2. Next, the long alkyl side chains that are linked to the fluorene (**2a**) or thiophene (**3a**-DP) units facilitate the polymers' solubility. In addition, the side chains may impede interchain interactions between the conjugated polymer backbones, decreasing the probability of exciton trapping/quenching by aggregate states.[7,12] Finally, the carboxylic acid groups are in close proximity to the BTD acceptor unit, and this may facilitate electronic coupling between the polymer and the TiO_2 surface facilitating charge injection.

The results presented herein demonstrate that the polymers perform well as sensitizers in the DSSC format, with maximum IPCE values obtained in excess of 60%, with a maximum power conversion efficiency of ~3% obtained. An important outcome of this work is the demonstration that the performance of the polymers in the DSSC varies with the DP. In particular, higher IPCE and power conversion efficiency are obtained for the polymer with the lowest DP. A study of the effect of polymer molecular weight on the TiO_2 adsorption shows that the effect arises because the lower molecular weight polymer adsorbs more effectively on the nanostructured film.

EXPERIMENTAL SECTION

Materials and Synthesis. All reagents were used as received unless otherwise specified. Tetrahydrofuran (THF) was distilled from sodium/benzophenone. 4,7-Dibromo-2,1,3-benzothiadizole[15] and 2,5-dibromo-3,4-dioctylthiophene were synthesized according to literature methods.[16] Detailed procedures for preparation of precursor compounds and copolymers are provided in the Supporting Information. All reactions were carried out under nitrogen or argon flow unless otherwise noted.

General Methods and Instrumentation. NMR spectra were obtained on a Varian Gemini instrument operating at 300 MHz with chloroform-*D* and/or dimethyl sulfoxide-D_6 as solvents. Gel permeation chromatography (GPC) analyses were conducted on a system comprised of a Rainin Dynamax SD-200 pump, Polymer Laboratories PLgel mixed D columns, and a Beckman Instruments Spectroflow 757 UV−visible absorption detector. The molecular weight was calibrated by using polystyrene standards. UV−vis absorption spectra were recorded on a Varian 50 Bio spectrophotometer. Emission spectra were recorded on a PTI QuantaMaster fluorescence spectrometer; the spectra are corrected for instrument response. Cyclic voltammetry was carried out on a computer-controlled CHI660A electrochemical workstation, where a glassy carbon electrode served as the working electrode, a platinum electrode as the counter electrode, and a silver disk as the reference electrode. Ferrocene (Fc) was used as an internal reference, a solution of tetrabutylammonium hexafluorophosphate (0.1 M) in dry dimethyl formamide (DMF) was used as the supporting electrolyte, and the scan rate was 100 mV-s^{-1}. Confocal fluorescence microscope images were obtained on a Zeiss Pascal LSM5 Confocal Laser Scanning Microscope.

DSSC Fabrication and Characterization. The cells were fabricated as a sandwich with fluorine-doped tin(IV) oxide (FTO) conducting glass, nanocrystalline TiO_2 as the wide bandgap semiconductor with the dyes adsorbed, I^-/I_3^- electrolyte for charge regeneration, and a Pt counter electrode as a catalyst. The TiO_2 paste, which was received as a gift from Dr. Felix N. Castellano at Bowling Green State University, was doctor-bladed onto a clean FTO glass slide and sintered at 450 °C for 30 min. The sintered electrode was immersed into the polymer solution in DMF (~0.2 mM, based on repeat units) for 24 h to allow for dye adsorption. The counter electrode was prepared by sputtering Pt on FTO glass with a thickness of 10 nm. Finally, an electrolyte solution containing 0.05 M I_2 and 0.1 M LiI in distilled propylene carbonate was drawn into the sandwich between the TiO_2 working electrode and the Pt counter electrode by capillary action. The active area of the cell was 0.90 cm^2.

The current−voltage characteristics of the cells were measured with a Keithley 2400 source meter under AM1.5 (100 mW/cm^2) solar simulator. For IPCE measurements, the cells were illuminated by monochromatic light from an Oriel Cornerstone spectrometer, and the current response under short circuit conditions was recorded at 10 nm intervals using a Keithley 2400 source meter. The light intensity at each wavelength was calibrated with an energy meter (S350, UDT Instruments).

RESULTS AND DISCUSSION

Polymer Synthesis and Characterization. The general synthetic routes to prepare **1**, **2a**, and **3a**-DPs are shown in Scheme S1 in the Supporting Information, and detailed syntheses and characterization data are provided therein as well. The neutral precursor polymers **2b** and **3b** with ester groups were synthesized

via a Suzuki cross-coupling reaction. Following the polymerization reaction, the polymers were purified and fractionated using preparative GPC with THF as an eluent. Importantly, precursor polymer **3b** was fractionated into three separate molecular weight fractions, that is, **3b-5**, **3b-8**, and **3b-11** (here, the trailing number refers to the DP; see below). Precursor **2b** was also purified by preparative GPC to remove low molecular weight impurities and catalyst. Following the separation and fractionation, the *t*-butyl ester protecting groups were removed by treatment with trifluoroacetic acid to afford carboxylic acid functionalized polymers **2a**, **3a-5**, **3a-8**, and **3a-11**.

The molecular weight and polydispersity index (PDI) of the neutral *t*-butyl ester polymers, that is, **2b** and **3b**-DPs, were determined by analytical GPC using polystyrene standards. The number average molecular weight (M_n) of the polymers varied from 4000 to 8800, with relatively small PDIs (1.2−1.6; see Table 1). The DP for each sample was calculated from the formula weight of the polymer repeat unit and M_n, and these values are also listed in Table 1, and the samples are labeled according to the DP. The ^{1}H NMR spectra of the polymers after removal of the ester units do not show the protons of *tert*-butyl groups, consistent with complete deprotection. In addition, the spectra of the acid forms of the polymers feature a weak resonance at $\delta \sim 12.8$ ppm attributed to the −COOH groups.

Optical Properties of the Polymers in Solution. The absorption and fluorescence spectra of the polymers were measured in DMF solution. The spectra are shown in Figure 1, and a tabulation of absorption and emission maxima, molar absorptivity values, and fluorescence quantum yields (ϕ_{fl}) is provided in Table 1. For comparison, the absorption and emission spectra of model oligomer **1** are also included. Oligomer **1** features a single absorption band with $\lambda_{max} \sim 380$ nm, whereas polymers **2a** and **3a** exhibit a two-band absorption, with a transition at $\lambda_{max} \sim 380$ nm and an additional band that appears in the mid-visible region. The two-band absorption is typical of D-A type conjugated polymers,[17,18] and the origin of the two transitions has recently been discussed by Reynolds and co-workers.[19] The dominant long wavelength band has considerable charge transfer character, where the electron-rich segment (fluorene or thiophene) serves as the donor, and the electron-deficient benzothiadiazole unit is the acceptor. Note that the visible transition is red-shifted in **3a** as compared to **2a**; this effect is due to the stronger donor strength (higher HOMO level) for the 3,4-dialkyl-2,5-thienylene unit as compared to the fluorene.[20] This red shift for **3a** is beneficial from the standpoint of visible light harvesting, as the absorption of this polymer overlaps better with the solar spectrum.

Table 1. Properties of Model Molecule and Polymers

	M_n[a]	PDI	DP	λ_{abs} (nm)	ε (10^4 cm^{-1} M^{-1})	λ_{em} (nm)	ϕ_{fl}[b]
1	388			380	0.8	556	0.39
2a	6400	1.60	7	372, 445	3.1	670	0.099
3a-5	3980	1.20	5	378, 466	1.3	731[c]	0.029
3a-8	6200	1.40	8	379, 472	1.4	733[c]	0.028
3a-11	8800	1.30	11	380, 476	1.2	733[c]	0.027

[a] Values determined from neutral precursor except **1**. [b] Determined using quinine sulfate in 0.1 M H_2SO_4 as the standard, $\phi_{fl} = 0.55$. [c] Estimated error in λ max is ±5 nm.

As described above, three samples of **3a** are available with DPs ranging from 5 to 11. As seen from the data in Table 1, there is only a slight red shift in wavelength maxima for the two absorption bands with increasing DP, from DP = 5 to 11. This finding suggests that the conjugation length of the polymer is nearly saturated for **3a-11**. We also note that the extinction coefficient (ε) at the absorption maximum for oligomer **1** is 0.8×10^4 cm^{-1} M^{-1}, while the values for the polymers are significantly larger, for example, 3.1×10^4 cm^{-1} M^{-1} for **2a** and 1.3×10^4 cm^{-1} M^{-1} for **3a**. Looking to the literature, there are several reports of D-A polymers with a similar structure as **3a**.[19,21] Interestingly, the absorption bands of **3a** are blue-shifted relative to the examples in the literature, and the long wavelength band is asymmetric with a "tail" on the long wavelength side. It is likely that the blue shift and asymmetry arise due to steric hindrance induced by the 3,3′-carboxyl groups that are present on the thienylene rings that flank the central benzothiadiazole unit. These substituents force the arylene rings out of a planar conformation, which disrupts to some extent π-conjugation and the D-A interaction.

Oligomer **1** and polymers **2a** and **3a** exhibit fluorescence in the visible region, and the spectra are collected in Figure 1b, and the quantum yields (ϕ) and emission maxima are listed in Table 1. Oligomer **1** features a strong green fluorescence with $\lambda_{max} \sim 556$ nm and a Stokes shift (peak to peak) of ca. 176 nm (~1.0 eV), indicating a strong intrachain charge transfer character in the singlet excited state of **1**.[6] The fluorescence from the polymers is red-shifted considerably as compared to the oligomer. Specifically, **2a** exhibits red fluorescence with $\lambda_{max} \sim 670$ nm, while **3a** exhibits weak fluorescence with $\lambda_{max} \sim 730$ nm. Both **2a** and **3a** exhibit Stokes shifts in excess of 200 nm (~1.0 eV). These large Stoke shifts suggest significant energy loss upon photoexcitation, which is likely due to the twisted thienylene−benzothiadiazole interaction and/or intramolecular charge transfer. The fluorescence quantum yields decrease significantly in the series **1** > **2a** ≫ **3a**. This trend is likely due in part to the energy gap law[22] but may also be due to increased charge transfer character inherent in the excited states of the polymers that fluoresce at longer wavelength.

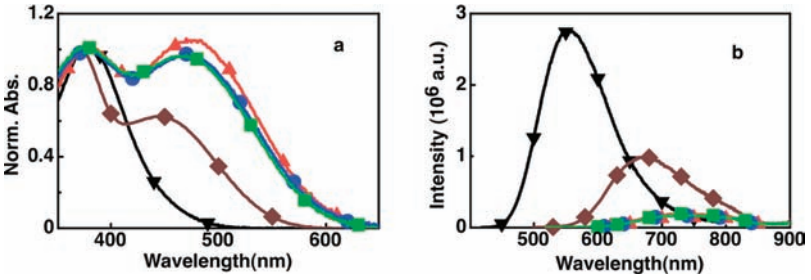

Figure 1. Absorption (a) and fluorescence (b) of **1** (black inverted triangle), **2a** (brown diamond), **3a-5** (green square), **3a-8** (blue circle), and **3a-11** (red triangle) in DMF, [RU] = 5 μM. The absorption spectra are normalized at the max of the near-UV band, while the fluorescence spectra are normalized according to their relative quantum yields.

dx.doi.org/10.1021/ja109926k | *J. Am. Chem. Soc.* 2011, 133, 3063–3069

Table 2. Electrochemical Properties of D-A Polymers

compound	E_{red} (V)[a] vs Fc^+/Fc	E_{0-0} (eV)[b]	E_{ox} (V)[c] vs Fc^+/Fc	E_{LUMO} (eV)[d]	E_{HOMO} (eV)[e]
1		2.65			
2a	−1.12	2.07	0.95	−3.68	−5.75
3a-11	−1.18	1.88	0.70	−3.62	−5.50
3a-8	−1.13	1.89	0.76	−3.67	−5.56
3a-5	−1.08	1.90	0.82	−3.72	−5.62

[a] Determined by cyclic voltammetry, Fc^+/Fc as an internal standard. [b] Optical bandgap, determined from the absorption onset. [c] Calculated from the equation: $E_{ox} = E_{0-0} - E_{red}$. [d] $E_{LUMO} = -(4.8 + E_{red})$ eV. [e] $E_{HOMO} = -(4.8 + E_{ox})$ eV.

Electrochemical Properties. The electrochemical properties of the oligomer and polymer samples were characterized using cyclic voltammetry in DMF solution. Each polymer exhibited irreversible cathodic waves upon cycling to negative potentials affording reduction potentials (E_{red}); however, anodic (oxidative) waves were not observed. Thus, the oxidation potentials (E_{ox}) were estimated by using the reduction potentials and the bandgap (E_{0-0}) via the relationship $E_{red} \sim E_{ox} - E_{0-0}$.[23] The values for the redox potentials are listed in Table 2 (relative to Fc/Fc^+), along with estimated HOMO and LUMO energies. The results show that the polymers have similar E_{red} values (−1.1 ∼ −1.2 V vs Fc^+/Fc); this correspondence is because the structures share the same BTD acceptor unit, which determines the LUMO level. These polymer E_{red} values are sufficiently negative as compared to the TiO_2 conduction band (−0.9 V vs Fc^+/Fc),[24] such that charge injection into the semiconductor is anticipated. The estimated E_{ox} values for **3a**-DP are less positive as compared to that of **2a**, which reflects the fact that thiophene is a stronger donor as compared to fluorene. Nevertheless, the oxidation potential for each of the polymers is sufficiently more positive than the redox potential of the iodine/iodide couple (0.24 V vs Fc^+/Fc).[25] This is significant because it indicates that the photo-oxidized polymers can be efficiently reduced by iodide. Taken together, the available electrochemical data confirm that there is a reasonable driving force for both electron injection and oxidized polymer regeneration in a DSSC format.

Polymer Adsorption on TiO_2 Films and Charge Injection. UV−visible absorption spectroscopy was used to monitor the adsorption of the oligomer **1** and polymers **2a** and **3a**-DP on nanocrystalline TiO_2 films. Prior to the adsorption, the absorption spectra of the sintered films were measured; each of the films used had a similar (weak) absorption (due to scattering) in the visible region, suggesting that the films were of comparable thickness. The TiO_2 films were immersed into DMF solutions of the materials for 24 h, and then, the absorption spectra of the resulting polymer (oligomer) adsorbed films were measured (Figure 2a, plots were corrected for background absorption/scattering by TiO_2). In each case, strong absorption is observed, indicating that a significant amount of each polymer adsorbs to the metal oxide surface. Adsorption presumably involves interaction between the TiO_2 surface and the carboxylic acid units in the polymers.[13] Qualitatively, the spectra of the adsorbed polymers are similar to their spectra in solution (compare Figure 1a). In particular, the film of **2a** exhibits strong absorption at $\lambda \sim 450$ nm, whereas polymers **3a**-DP absorb at longer wavelength. Note that the two-band profile observed for **3a**-DP is not well resolved for the film, possibly due to structural (conformational) heterogeneity for the adsorbed polymer. Note

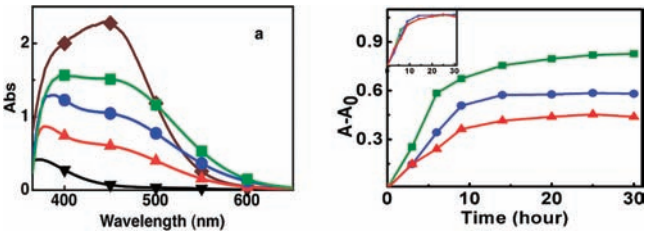

Figure 2. Absorption spectra after dye deposition for 24 h (a) and time-dependent adsorption (b) of **1** (black inverted triangle), **2a** (brown diamond), **3a-11** (red triangle), **3a-8** (blue circle), and **3a-5** (green square) on TiO_2 films. A_0, absorbance of film without dye at 450 nm; A, absorbance of film with dye at 450 nm (only for **3a**-DPs). The inset in b shows adsorption plots for **3a**-DPs normalized at $t = 25$ h.

that the film of **1** exhibits a relatively weak absorption that is consistent with its smallest extinction coefficient that gives rise to the lowest absorbance on TiO_2 film. When comparing the absorption of the polymer adsorbed films, it can be seen that the absorption strength varies in the sequence, **2a** > **3a-5** > **3a-8** > **3a-11**. The largest absorption for **2a** is explained by the fact that this polymer has a larger molar absorptivity as compared to the **3a**-DP series (3.1×10^4 vs $\sim 1.3 \times 10^4$ M^{-1} cm^{-1}).

The most interesting result of the film adsorption experiments is that absorbance of the **3a**-DP series varies with polymer chain length. These results strongly suggest that the amount of polymer **3a**-DP that adsorbs to the nanocrystalline TiO_2 *increases with decreasing polymer chain length*. To better understand the effect of polymer chain length on the adsorption process, the time dependence of the absorption of a series of films soaked in the polymer solutions for varying time was determined, and the results are shown Figure 2b. These data reveal that for each polymer sample, the absorption increases over a 20 h period and then levels off, indicating saturation. The data indicate that the rate of adsorption does not vary strongly with polymer chain length (see inset in Figure 2b); however, consistent with the spectra in Figure 2a, the final absorption increases substantially with decreasing chain length. Because the molar absorptivity for the **3a**-DP series does not vary with chain length (when expressed per repeat unit), the absorption data demonstrate that the amount of polymer that absorbs to the nanocrystalline TiO_2 film increases with decreasing polymer chain length.

Evidence that the **3a**-DP undergoes charge injection when it is adsorbed on TiO_2 comes from time-resolved fluorescence spectroscopy, which provides evidence for fluorescence quenching on at the metal oxide surface. Specifically, the fluorescence decay kinetics of **3a-5** in DMF solution and adsorbed on silica are very similar, with median lifetimes of 1.74 and 1.58 ns, respectively. However, on TiO_2, the fluorescence decays much more rapidly, with a median lifetime of 0.76 ns. This result indicates that ≥50% of the singlet excitons are quenched at the TiO_2 interface. To provide more insight regarding the nature of the exciton quenching, nanosecond transient absorption studies were carried out for the polymer-coated TiO_2 films to investigate the efficiency of charge injection and regeneration. The films were immersed in degassed propylene carbonate, and they were subjected to 420 nm excitation pulses (∼5 ns pulse width). Immediately following excitation, strong transient absorption was observed for all of the materials (Figure S-2 in the Supporting Information). For example, a **3a-5**-coated film shows a broad absorption at $\lambda > 570$ nm with an absorption maximum at ca. 750 nm. This transient absorption is attributed to the oxidized

dx.doi.org/10.1021/ja109926k | *J. Am. Chem. Soc.* 2011, 133, 3063–3069

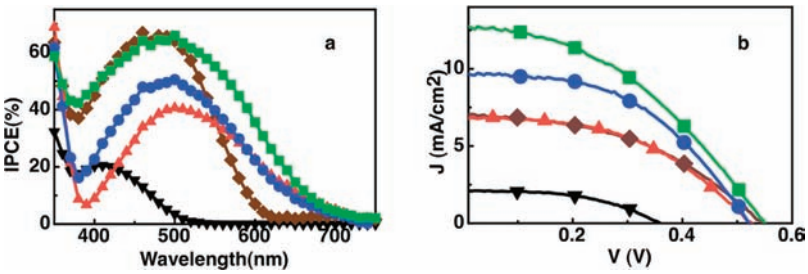

Figure 3. Photocurrent action spectra (a) and $J-V$ characteristics (b) of cells made from **1** (black inverted triangle), **2a** (brown diamond), **3a-11** (red triangle), **3a-8** (blue circle), and **3a-5** (green square). The electrolyte solution is composed of 0.05 M I_2 and 0.1 M LiI in propylene carbonate.

Table 3. Summary of Solar Cell Characteristics under AM1.5 Illumination

	V_{oc} (V)	J_{sc} (mA/cm^2)	FF (%)	maximum IPCE (%)	η_{cell} (%)
1	0.36	2.12	49.1	20.1	0.375
2a	0.55	7.02	43.8	65.8	1.68
3a-11	0.52	6.80	47.5	40.0	1.70
3a-8	0.52	9.82	47.5	50.0	2.45
3a-5	0.54	12.58	44.9	65.1	2.99

polymer cation (positive polaron), which is produced by photoinduced charge injection into the TiO_2 conduction band.[26] The polymer cation signal decays with a ca. 325 μs lifetime due to charge recombination between the cation and the TiO_2 conduction band electrons. Similar results were obtained for adsorbed films of the other polymer samples; however, the amplitude of the transient absorption varied in the order **3a-11** < **3a-8** < **3a-5**, suggesting that the charge injection yield decreases with increasing polymer chain length. When the polymer-adsorbed TiO_2 films are immersed in I_3^-/I^- solution, the transient absorption is substantially quenched (see **3a-5** as an example in Figure S-3 in the Supporting Information). This result indicates that the oxidized dye cation state is efficiently reduced by electron transfer from iodide, resulting in efficient regeneration of the reduced polymer following photoinduced charge injection.[25]

Polymer-Sensitized Solar Cell Characterization. The polymer-coated TiO_2 films were tested in a standard DSSC format using a propylene carbonate solution of I_2/LiI as the electrolyte and a Pt/FTO counter electrode. Figure 3a illustrates the photocurrent action spectra (IPCE) of the polymer-sensitized solar cells obtained using monochromatic illumination under short circuit conditions. The trend of peak efficiency is in qualitative agreement with the absorption spectra of the films (Figure 2a). In particular, the DSSC cell fabricated with **1** has the lowest peak external quantum efficiency of ca. 20%, whereas the cells from **2a** and **3a**-DPs have maximum IPCE values in the 40−60% range. In addition, the IPCE response extends into the near-infrared region for the **3a**-DPs, whereas the photocurrent response for **2a** is nil for λ > 600 nm. Importantly, the peak IPCE observed for **2a** and **3a-5** is greater than 60%, indicating that at short-circuit photoinduced charge injection is quite efficient for the polymer sensitizers.

The most significant point with respect to the IPCE data in Figure 3a is the fact that the maximum IPCE for the **3a**-DP series *decreases* with *increasing* chain length (i.e., **3a-5** > **3a-8** > **3a-11**). This result is consistent with the polymer/TiO_2 adsorption study (Figure 2), which shows that the amount of **3a**-DP that is adsorbed to the nanostructured TiO_2 film decreases with increasing polymer chain length. Thus, the trend in IPCE values appears to result from the difference in light-harvesting efficiency for the films prepared from the polymers with different chain length.

The $J-V$ characteristics under AM1.5 illumination (100 mW-cm^{-2}) of the polymer sensitized DSSCs are shown in Figure 3b. The performance of the cells in terms of short-circuit current density (J_{sc}), open-circuit voltage (V_{oc}), fill factor (FF), and overall power conversion efficiency (η_{cell}) are summarized in Table 3, along with the maximum IPCE values. The photovoltaic parameters (J_{sc}, V_{oc}, FF, and η_{cell}) of the cell made from oligomer **1** are 2.12 mA cm^{-2}, 0.36 V, 0.491, and 0.375%. In contrast, the cells made from polymer dyes have significantly enhanced performance. For example, J_{sc}, V_{oc}, FF, and η_{cell} of **2a** are 7.02 mA cm^{-2}, 0.55 V, 0.438, and 1.68%, respectively. Both V_{oc} and J_{sc} increase considerably, suggesting that there are advantages for using D-A polymers rather than using small molecular dyes. These advantages include a broadened absorption spectrum (an increase in light harvesting efficiency) and enhanced charge injection efficiency. When the fluorene unit is replaced with thiophene in the conjugated polymer backbone, an additional increased photocurrent of **3a**-DPs is observed relative to **2a**. The optimum performance for **3a**-DPs is from the cell of **3a-5** with a large J_{sc} value of 12.58 mA cm^{-2} and η_{cell} of 2.99%. This represents the highest reported efficiency for a polymer-sensitized DSSC using I_3^-/I^- electrolyte without any other additives such as ionic liquids,[13] or *tert*-butyl pyridine.[10] However, a relatively low FF (0.449) indicates that future efforts are needed to modify device fabrication methods and enhance the charge collection efficiency.[26]

Importantly, the results of the AM1.5 studies are parallel with the IPCE results in showing that the overall photocurrent and power conversion efficiency for the **3a**-DP series *increases* with *decreasing* polymer chain length. This result confirms the trends noted above and clearly demonstrates that the overall efficiency of the polymer-sensitized DSSCs is optimal for relatively low polymer chain length.

Confocal Fluorescence Microscopy and Chain Length Dependence of Polymer Adsorption. The results of the polymer adsorption and solar cell testing show that the polymer chain length has a strong effect on the amount of the **3a**-DP that adsorbs to the mesoporous TiO_2 films. We hypothesized that the shorter chain length polymer is better able to penetrate the mesoporous structure, resulting in improved adsorption of the polymer onto the mesoporous film. Thus, to explore the effective penetration of the polymer into the TiO_2 film, confocal microscopy was applied to probe the fluorescence intensity as a function of depth.[27]

A set of three TiO_2 films prepared at the same time and nominally having the same thickness were used to adsorb the

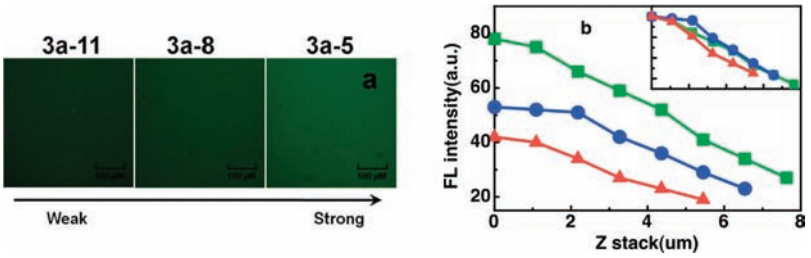

Figure 4. Confocal fluorescence microscopy of top view (a) and Z stack scan with inset of normalized intensities (b) of **3a-11** (red triangle), **3a-8** (blue circle), and **3a-5** (green square) on TiO_2 films. Excitation laser wavelength, 488 nm.

polymer samples with different DPs, **3a-11**, **3a-8**, and **3a-5**. The films were then interrogated using a confocal microscope, with excitation at 488 nm and monitoring the red fluorescence from the adsorbed polymer. Figure 4a compares the fluorescence images obtained with the focal plane approximately at the film/air interface for films that are adsorbed using **3a-11**, **3a-8**, and **3a-5**. (Note that in Figure 4a the green is a "false color", but the brightness of the image represents the relative fluorescence intensity.)

It is evident from this presentation that the fluorescence intensity increases in order **3a-11** < **3a-8** < **3a-5**. Because the three polymer samples have the same fluorescence quantum yield (Table 1), the brightness is proportional to the relative amount of polymer adsorbed on the TiO_2 film.[27] Thus, this result is consistent with the optical data presented above in indicating that the amount of polymer adsorbed increases as the polymer chain length decreases. Next, Figure 4b illustrates the fluorescence intensity as monitored as the confocal image plane is sequentially moved through the depth of the TiO_2 film (*z*-stack). As can be seen, for each of the films, the intensity decreases approximately linearly with depth into the TiO_2 films. Comparing the plots for the different polymer samples again reveals that the intensity decreases with increasing polymer chain length, indicating the amount of polymer adsorbed decreases with increasing chain length. The inset of Figure 4b shows the superimposed depth scans for the three samples, normalized to the intensity at the air/film interface. This presentation indicates that the relative variation in intensity as a function of depth into the film is approximately the same for the three polymer samples. This result suggests that the ability of the polymers to penetrate into the interior of the TiO_2 film is approximately the same; we conclude the difference in amount adsorbed for the different chain length samples is due to another factor.

Given this result, we suggest that the chain length dependence of the adsorption results from the *nanoporous* structure of the TiO_2. Previous studies of the porosity of nanostructured TiO_2 aerogels indicate that much of the available surface area exists within pores having a diameter <100 Å, with a substantial fraction in pores <25 Å.[28,29] The end-to-end chain length of the **3a**-DP series of polymers falls in the range ~60−95 Å. In view of this polymer chain size, and the fact that a substantial fraction of pores fall in the same size range, it seems likely that the TiO_2 acts as a nanoporous size-exclusion material, effectively partitioning polymer chains by molecular weight. The result is that the smaller chains are able to access a greater fraction of the TiO_2 surface for adsorption, leading to the observed greater surface coverage. By contrast, the longer chains are excluded from a substantial fraction of the surface because they cannot effectively penetrate into the smaller pores, and consequently,this material is not able to give rise to as much surface coverage.

SUMMARY AND CONCLUSIONS

A set of two D-A type conjugated polymers with carboxylic acid side groups have been synthesized and utilized as active materials for DSSCs. The polymers feature a backbone consisting of an electron-poor BTD (acceptor) unit, alternating with either a thiophene−fluorene−thiophene triad (**2a**) or a terthiophene (**3a**-DP) segment as the donor. The alternating D-A structure embues the polymers with a comparatively low HOMO−LUMO gap, resulting in a broad and intense absorption throughout the mid-visible region. The absorption of **3a** is red-shifted as compared to that of **2a**, reflecting the stronger donor properties of the terthiophene segment.

The carboxylic acid units act as "anchors",[30] allowing the polymers to adsorb to the surface of TiO_2 from polar organic solvents. Time-dependent adsorption experiments show that adsorption of the polymers to the TiO_2 surface is complete in ~24 h. Semipreparative GPC afforded three samples of **3a** with different chain lengths, and interestingly, it was found that the amount of polymer that adsorbs increases with decreasing polymer chain length, with the sample having a DP of ~5 repeats giving the highest adsorption. Depth sampling of the polymer adsorbed TiO_2 films by using confocal fluorescence microscopy reveals that chain length does not influence the penetration of the polymer on the microscale. We conclude that the chain length dependences result from a difference in the ability of the polymers to diffuse through nanometer-scale pores in the nanostructured films. In essence, the shorter chain polymers are able to diffuse to and access regions of the film, which are inaccessible to polymers with a larger average chain length.

Photoelectrochemical cells based on the DSSC format were fabricated using the polymers as sensitizers. The cells constructed using the polymers exhibit a considerably higher peak IPCE than those that use a D-A oligomer as the dye (**1**), approximately 65% for both **2a** and **3a-5**, with the oligomer giving just over 20% peak IPCE. The DSSC that is based on the low molecular weight polymer sample **3a-5** exhibits the best performance, with J_{sc} of 12.58 mA cm^{-2}, V_{oc} of 0.53 V, FF of 44.9%, and η_{cell} of 2.99%. This efficiency is the highest value that has been reported for a DSSC, which incorporates a conjugated polymer as the sensitizer without specific optimization such as the use of solution modifiers or light-scattering layers.[10,26]

In conclusion, we note that several recent studies of conjugated polymer based bulk heterojunction solar cells have demonstrated a correlation between polymer chain length and device performance. These studies have shown that performance *increases* with polymer molecular weight, with an optimum reached for samples having M_n > 25 kDa.[31,32] In these systems, the effect of polymer chain length is believed to arise due to increased structural order in the bulk heterojunction films. In this study of

polymer-sensitized DSSCs, we demonstrate an inverse correlation between polymer chain length and cell performance. Although the underlying basis for the dependence on polymer chain length is entirely different in the two solar cell configurations, the effects seen in these conjugated polymer-based systems underscore the important relationship between polymer structure and performance in solar cell applications. It is likely that in future work it will be possible to use polymer synthetic methods to control and optimize the structure and chain length of the carboxylic acid-functionalized D-A conjugated polymers for applications in hybrid cell format.

■ ASSOCIATED CONTENT

Supporting Information. Detailed description of synthesis and spectral characterization of polymers, polymer cyclic voltammetry, transient absorption of polymer-TiO_2 films, and fluorescence decays (1 Scheme, 4 Figures). This material is available free of charge via the Internet at http://pubs.acs.org.

■ AUTHOR INFORMATION

Corresponding Author
kschanze@chem.ufl.edu

■ ACKNOWLEDGMENT

We thank the U.S. Department of Energy (Grant DE-FG02-03ER15484) for support of this work. We also thank Dr. Felix N. Castellano at Bowling Green State University for providing the TiO_2 paste.

■ REFERENCES

(1) O'Regan, B.; Grätzel, M. *Nature* **1991**, *353*, 737.
(2) Grätzel, M. *Inorg. Chem.* **2005**, *44*, 6841.
(3) Chiba, Y.; Islam, A.; Watanabe, Y.; Komiya, R.; Koide, N.; Han, L. *Jpn. J. Appl. Phys. Part 2* **2006**, *45*, L638.
(4) Zeng, W.; Cao, Y.; Bai, Y.; Wang, Y.; Shi, Y.; Zhang, M.; Wang, F.; Pan, C.; Wang, P. *Chem. Mater.* **2010**, *22*, 1915.
(5) Bessho, T.; Zakeeruddin, S. M.; Yeh, C.-Y.; Diau, E. W.; Grätzel, M. *Angew. Chem., Int. Ed.* **2010**, *49*, 6646.
(6) Zhao, X.; Pinto, M. R.; Hardison, L. M.; Mwaura, J.; Muller, J.; Jiang, H.; Witker, D.; Kleiman, V. D.; Reynolds, J. R.; Schanze, K. S. *Macromolecules* **2006**, *39*, 6355.
(7) Mwaura, J. K.; Zhao, X.; Jiang, H.; Schanze, K. S.; Reynolds, J. R. *Chem. Mater.* **2006**, *18*, 6109.
(8) Kim, Y. G.; Walker, J.; Samuleson, L. A.; Kumar, J. *Nano Lett.* **2003**, *3*, 523.
(9) Liu, Y.; Summers, M. A.; Edder, C.; Frechet, J. M. L.; McGehee, M. D. *Adv. Mater.* **2005**, *17*, 2960.
(10) Zhang, W.; Fang, Z.; Su, M.; Saeys, M.; Liu, B. *Macromol. Rapid Commun.* **2009**, *30*, 1533.
(11) Senadeera, G. K. R.; Nakamura, K.; Kitamura, T.; Wada, Y.; Yanagida, S. *Appl. Phys. Lett.* **2003**, *83*, 5470.
(12) Jiang, H.; Zhao, X.; Shelton, A. H.; Lee, S. H.; Reynolds, J. R.; Schanze, K. S. *ACS Appl. Mater. Interfaces* **2009**, *1*, 381.
(13) Cheng, Y.-J.; Yang, S.-H.; Hsu, C.-S. *Chem. Rev.* **2009**, *109*, 5868.
(14) Kanimozhi, C.; Balraju, P.; Sharma, G. D.; Patil, S. *J. Phys. Chem. C* **2010**, *114*, 3287.
(15) Zoombelt, A. P.; Fonrodona, M.; Wienk, M. M.; Sieval, A. B.; Hummelen, J. C.; Janssen, R. A. J. *Org. Lett.* **2009**, *11*, 903.
(16) Banishoeib, F.; Henckens, A.; Fourier, S.; Vanhooyland, G.; Breselge, M.; Manca, J.; Cleij, T. J.; Lutsen, L.; Vanderzande, D.; Nguyen, L. H.; Neugebauer, H.; Sariciftci, N. S. *Thin Solid Films* **2008**, *516*, 3978.
(17) Herguth, P.; Jiang, X.; Liu, M. S.; Jen, A. K.-Y. *Macromolecules* **2002**, *35*, 6094.
(18) Wu, P.-T.; Kim, F. S.; Champion, R. D.; Jenekhe, S. A. *Macromolecules* **2008**, *41*, 7021.
(19) Beaujuge, P. M.; Amb, C. M.; Reynolds, J. R. *Acc. Chem. Res.* **2010**, *43*, 1396.
(20) Beaujuge, P. M.; Ellinger, S.; Reynolds, J. R. *Nat. Mater.* **2008**, *7*, 795.
(21) Beaujuge, P. M.; Subbiah, J; Choudhury, K. R.; Ellinger, S.; McCarley, T. D.; So, F.; Reynolds, J. R. *Chem. Mater.* **2010**, *22*, 2093.
(22) Henry, B. R.; Siebrand, W. In *Organic Molecular Photophysics*; Birks, J. B., Ed.; Wiley: New York, 1973; Vol. I.
(23) The energy gap (E_{0-0}) was calculated through the equation, $E_{0-0} = 1240/\lambda_{onset}$.
(24) Hagfeldt, A.; Gratzel, M. *Chem. Rev.* **1995**, *95*, 49.
(25) Lenzmann, F.; Krueger, J.; Burnside, S.; Brooks, K.; Gratzel, M.; Gal, D.; Ruhle, S.; Cahen, D. *J. Phys. Chem. B* **2001**, *105*, 6347.
(26) Wang, P.; Zakeeruddin, S. M.; Moser, J. E.; Humphry-Baker, R.; Grätzel, M. *J. Am. Chem. Soc.* **2004**, *126*, 7164.
(27) Because the resolution of the confocal microscope is <1 μm along the *z*-direction, the fluorescence intensity depth profile provides insight regarding the relative surface concentration of **3a**-DP on the micrometer length scale as a function of depth in the TiO_2 film. Here, we assume that the fluorescence intensity of the surface-adsorbed polymer reflects its surface concentration within the film.
(28) Papageorgiou, N.; Barbe, C.; Grätzel, M. *J. Phys. Chem. B* **1998**, *102*, 4156.
(29) Zhu, Z.; Tsung, L. Y.; Tomkiewicz, M. *J. Phys. Chem.* **1995**, *99*, 15945.
(30) Rochford, J.; Chu, D.; Hagfeldt, A.; Galoppini, E. *J. Am. Chem. Soc.* **2006**, *129*, 4655.
(31) Coffin, R. C.; Peet, J.; Rogers, J.; Bazan, G. C. *Nature Chem.* **2009**, *1*, 657.
(32) Bijleveld, J. C.; Zoombelt, A. P.; Mathijssen, S. G. J.; Wienk, M. M.; Turbiez, M.; Leeuw, D. M.; Janssen, R. A. J. *J. Am. Chem. Soc.* **2009**, *131*, 16616.